Electrochemistry

DOI: 10.1002/ange.201302704

Generation of Electricity and Illumination by an Environmental Fuel Cell in Deep-Sea Hydrothermal Vents**

Masahiro Yamamoto, Ryuhei Nakamura,* Kazumasa Oguri, Shinsuke Kawagucci, Katsuhiko Suzuki, Kazuhito Hashimoto, and Ken Takai*

Public interest in the generation of power by alternative energy sources in the ocean beyond fossil fuels and nuclear energy has increased in recent years.[1–4] Power generation in the ocean is also of great interest for the inexpensive and efficient supply of electricity for the survey and exploration of submarine resources. Deep-sea hydrothermal vents are environments that discharge crustal hydrothermal fluids, geologically driven by magmatism and geochemically processed by the high temperatures of rock–seawater interactions and alterations.[5,6] Hydrothermal fluids enriched with reduced chemicals are mixed with oxidative chemicals in seawater in the vicinity of deep-sea vents. The steep chemical slope between the hydrothermal fluids and ambient seawater has the potential to generate electricity.[7] Therefore, it is likely that electricity is generated in situ between hydrothermal fluids (HF) and seawater (SW), which can be promoted and confirmed by deployment of artificial electrodes and a conductor. Herein, we show the development of an HF–SW fuel cell for deep-sea hydrothermal vents.

During the Integrated Ocean Drilling Program (IODP) in 2010,[8] several artificial hydrothermal vents were created by the drilling of wells in the Iheya North hydrothermal field[9] of the Okinawa Trough, Japan. One of the artificial hydrothermal vents (C0014G) had a vigorous discharge with a high fluid temperature ($T_{max} = 309\,°C$) at a water depth of 1053 m. In this work, seafloor electrochemical analyses were conducted in the C0014G vent using a remotely operated vehicle (ROV) equipped with a deep-sea potentiostat/galvanostat system (D-Pote), which was covered with an anti-pressure housing and controlled by an onboard computer through data communication.

First, the oxidation–reduction potential (ORP) of the ambient seawater and hydrothermal fluids was measured (Figure 1). The average temperature and ORP of the ambient seawater were approximately 4 °C and +478 mV, respectively, versus the standard hydrogen electrode (SHE), while those of the hydrothermal fluids were approximately 309 °C and −39 mV, respectively (Table 1). A difference of 0.52 V was observed between the hydrothermal fluids and the seawater, which provided the basis for establishing the generating capacity of the HF–SW fuel cell. The direct measurement of the in situ ORP in the hydrothermal fluids is valuable for understanding the environment. After removal

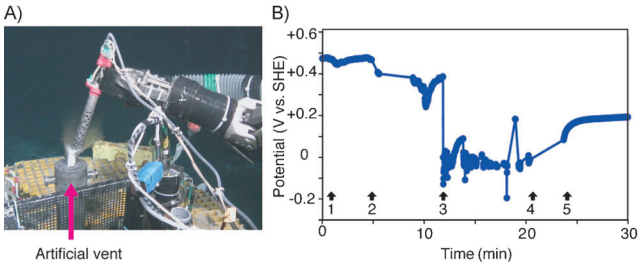

Figure 1. In situ measurement of the oxidation–reduction potential in hydrothermal fluids and ambient seawater. A) Photograph showing the measurement of the ORP in the hydrothermal fluids at the artificial vent site. A platinum working electrode was fixed in a perforated stainless-steel pipe and inserted into the hydrothermal fluids. B) Change in the ORP value during the ROV dive. The measuring points are shown as closed circles. The arrows indicate the times when 1) the ROV was above the vent, 2) the ROV landed on the seafloor beside the vent, 3) the anode was inserted into the hydrothermal fluids, 4) the anode was removed from the hydrothermal fluids, and 5) the ROV left from the vent.

Table 1: Physical, chemical, and electrochemical properties of the ambient seawater (SW) and hydrothermal fluids (HF) at the C0014G vent site in the Iheya North Field.

	SW	HF
T [°C]	4[a]	309[a]
pH	7.0[a]	4.8[a]
H_2 [μmol L^{-1}]	1.4[c]	230[b]
H_2S [μmol L^{-1}]	28[c]	4500[b]
O_2 [μmol L^{-1}]	65[a]	–
ORP [mV]	+478[a]	−39[a]
E' [mV]	+829[d]	−271[f]
	−125[e]	−71[e]

[a] Measured in this work. [b] Measured in previous work.[13] [c] Calculated from the dilution ratio of HF and SW by magnesium concentration. [d–f] Calculated from the half-reactions: [d] $O_2 + 4H^+ + 4e^- \rightleftarrows 2H_2O$; [e] $S + 2H^+ + 2e^- \rightleftarrows H_2S$; and [f] $2H^+ + 2e^- \rightleftarrows H_2$.

[*] Dr. M. Yamamoto, Dr. K. Oguri, Dr. S. Kawagucci, Dr. K. Suzuki, Dr. K. Takai
Japan Agency for Marine-Earth Science and Technology (JAMSTEC)
2-15 Natsushima-cho, Yokosuka 237-0061 (Japan)
E-mail: myama@jamstec.go.jp
Dr. R. Nakamura
RIKEN Center for Sustainable Resource Science
2-1 Hirosawa, Wako, Saitama 351-0198 (Japan)
E-mail: ryuhei.nakamura@riken.jp
Prof. K. Hashimoto
Department of Applied Chemistry, The University of Tokyo
7-3-1 Hongo, Bunkyo-ku, Tokyo 113-8656 (Japan)

[**] We are grateful to the captain, crew, and technical staff of the R/V Natsushima NT12-27 cruise for their technical expertise.
Supporting information for this article is available on the WWW under http://dx.doi.org/10.1002/anie.201302704.

of the working electrode from the hydrothermal fluids, the ORP increased, but did not recover to the value of the ambient seawater because of the precipitation of sulfide minerals that cover the surface of the electrode.

The equilibrium potentials (E'; Table 1) were theoretically calculated from the measured or estimated concentrations of the representative dissolved chemicals and the Gibbs free energy ($\Delta G°$) of the half-reactions in the ambient seawater and the hydrothermal fluids. The $\Delta G°$ values were computed by the SUPCRT program[10] (see the Supporting Information). There is a large gap between the two E' values estimated from the concentrations of dissolved O_2 (+829 mV) and H_2S (−125 mV) in the ambient seawater. The measured value of the ORP in the ambient seawater (+478 mV) is different from both of the calculated E' values. This result implies that the ambient seawater is the mixing and disequilibration zone between the hydrothermal fluids and the seawater, and direct measurement of the ORP is required. The measured value of the ORP in the hydrothermal fluids (−39 mV) was similar to the theoretical E' value, calculated from the dissolved H_2S (−71 mV) but not from the dissolved H_2 (−271 mV; Table 1). This result could be explained by the higher concentration of H_2S compared to the other reductive chemicals (i.e., H_2, CH_4, Fe^{2+}, and Mn^{2+}) in the hydrothermal fluids. The successful direct measurement of the ORP of the high-temperature hydrothermal fluids clearly indicates that the in situ ORPs of the hydrothermal fluids can be approximately estimated from the conditions (i.e., temperature, pH value, and concentration of dissolved H_2S), because many of the hydrothermal fluids are dominated by H_2S. However, because various types of hydrothermal fluids, such as H_2-abundant, CH_4-abundant, and Fe^{2+}-dominated hydrothermal fluids, exist in global deep-sea hydrothermal systems, the direct measurement of the in situ ORP would be valuable.

Next, we performed cyclic voltammetry (CV) on the ambient seawater and hydrothermal fluids at the C0014G vent site (Figure 2). To remove the contribution of the capacitive current, the averaged curves of the backward and forward scans are also depicted in Figure 2. The cathodic current exceeded the anodic current at a potential lower than +320 mV in the seawater (blue line, Figure 2A), which mainly results from the reduction of O_2 to water and/or the reduction of Fe^{3+} to Fe^{2+} dissolved in the seawater. By contrast, the anodic current exceeded the cathodic current at a potential higher than −120 mV in the hydrothermal fluids (red line, Figure 2B). Based on the theoretical calculation of the E' values, the anodic current is most likely produced by oxidation of H_2 and subsequently increased by oxidation of H_2S (Table 1). The difference between the two values (i.e., +320 mV and −120 mV) indicates that the open-circuit voltage (V_{oc}) is 0.43 V when the ambient seawater and hydrothermal fluids are connected by platinum electrodes. A comparison of the average change of 0.43 V in the current density (from −120 to +320 mV) from the reduction in the seawater (0.83 $A\,m^{-2}\,V^{-1}$) and the oxidation in the hydrothermal fluids (3.5 $A\,m^{-2}\,V^{-1}$) indicates that the oxidation reaction in the hydrothermal fluids is approximately 4.2 times faster than the reduction reaction in the seawater. This result

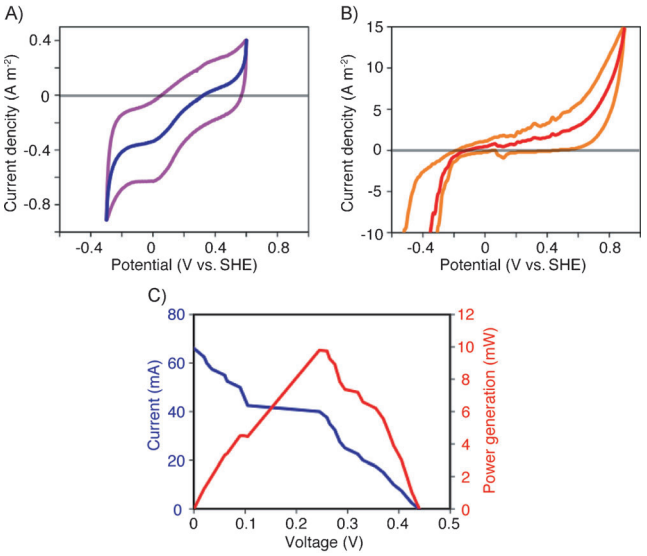

Figure 2. Electrochemical properties of SW and HF determined by voltammetry methods. A) Cyclic voltammetry in ambient seawater. The scan rate was 200 $mV\,s^{-1}$. The voltammogram is represented by a purple line, and the averaged curve of the backward and forward scans is represented by a blue line. B) Cyclic voltammetry in the hydrothermal fluids. The voltammogram and the averaged curve are represented by orange and red lines, respectively. C) The current and power curves for the HF–SW fuel cell using 0.05 m^2 of Pt anode and 0.4 m^2 of Pt cathode. The blue line indicates the current, and the red line indicates power generation.

implies that current generation would be regulated by the slower reduction reaction of O_2 on the platinum cathode when the SW cathode and the HF anode have the same surface area. We calculated the current generation efficiency (shown as a power curve in Figure 2C) with the surface areas of the anode and the cathode set to 0.05 m^2 and 0.4 m^2, respectively. These surface areas were the same as the total projected areas of electrodes in the HF–SW fuel cell we actually constructed (see next paragraph). The maximum power was estimated to be 9.8 mW (Figure 2C).

We designed and constructed an HF–SW fuel cell (Figure 3A). The cathode was composed of a platinum-coated titanium mesh board (50 cm × 50 cm, 0.40 m^2 of total projected area; Figure 3B). The anode was composed of a titanium pipe in which iridium-coated titanium mesh boards (40 cm × 1.5 cm × 5 pieces, 0.05 m^2 of total projected area) were fitted (Figure 3B). Iridium can catalyze the oxidation of H_2S in a manner similar to that of platinum (Figure 4). Three light-emitting diodes (LEDs) were connected between the cathode and the anode as the load. The ROV was equipped with these electrodes and the load. When the anode pipe was inserted into the high-temperature hydrothermal fluids at the C0014G vent, all of the LED lamps were illuminated (Figure 3C and D; a movie is also available in the Supporting Information). At least 5, 10, and 21 mW of electric power are required for the illumination of one, two, and three of the LEDs, respectively. The maximum power of the fuel cell, predicted from the surface area of the electrodes, was estimated to be 9.8 mW (Figure 2C). However, the fuel cell generated more than 21 mW of power. The

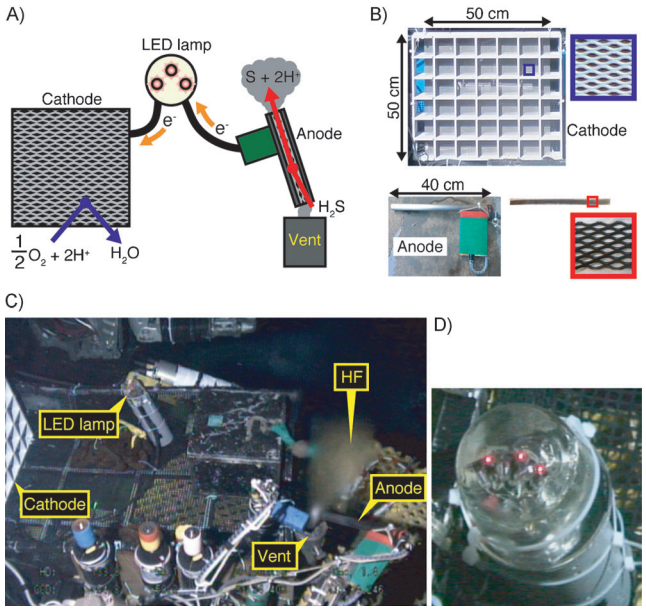

Figure 3. HF–SW fuel cell installed at a deep-sea hydrothermal vent and generation of electricity. A) A schematic illustration of the HF–SW fuel cell. When the hydrothermal fluids passes through the inside of the anode pipe, the anodic current is generated by oxidation of H_2S. The cathodic current is generated by reduction of O_2 in the ambient seawater on the cathode. The load (in this case, the LED lamp) was connected between the two electrodes for illumination. B) Photographs of the cathode and anode. The cathode is a platinum-coated titanium mesh board (50 cm long, 50 cm wide, 0.1 cm height). The anode is made of a titanium pipe ($\phi 3 \times 40$ cm) in which five pieces of iridium-coated titanium mesh boards (40×1.5 cm/piece) are fitted. Close-up photographs of mesh boards were shown in squares. C) A photograph taken by a camera located above the payload of the ROV. The anode of the fuel cell is inserted into the hydrothermal fluids. D) Close-up photograph of the LED lamp showing that all the red lights were illuminated.

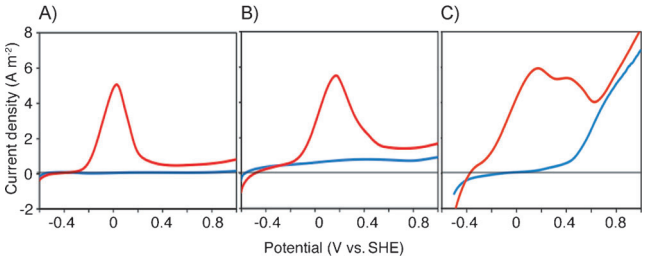

Figure 4. Linear-sweep voltammetry (LSV) in the laboratory. Platinum plate (A), iridium plate (B), and a plate of natural chimney minerals (C) were tested as the working electrode. The electrolytes contained NaCl (0.6 M) in the presence (red line) and absence (blue line) of Na_2S (0.1 M).

actual surface area of electrodes must thus be larger than the projected area because of the uneven surface of the mesh boards. The generated power is at least 21 mW (0.42 $W m^{-2}$ of anode), which is higher than that of any previously reported benthic microbial fuel cell ($\approx$0.25 $W m^{-2}$ of anode).[11,12] The LEDs were also illuminated when we employed the fuel cell at a natural hydrothermal vent site. This result was not surprising because no significant difference in the temperature and chemical components of the hydrothermal fluids was observed in the natural and artificial hydrothermal vents.

High-temperature hydrothermal fluids often form massive sulfide mineral structures called chimneys in and around the flow passages.[13] After the onboard recovery of the equipment, we observed sulfide minerals precipitated onto the surface of the anode inserted into the hydrothermal fluids. It has been demonstrated that precipitates of hydrothermal sulfide minerals can become excellent electrodes because of their conductivity and catalytic properties.[7,14] The sulfide chimney could catalyze the oxidation of H_2S in a manner similar to the platinum electrodes (Figure 4). In addition, the structure of the sulfide chimney itself serves as an electron donor through self-decomposition (Figure 4). These results strongly suggest that the anode inserted into the high-temperature hydrothermal fluids can preserve its function and performance because the anode surface is not easily covered with precipitates of sulfide minerals as a result of self-decomposition; even if the surface of the anode is completely covered with sulfide minerals, it has the ability to act as an anode.

In this work, we successfully generated electricity from deep-sea hydrothermal vents using a fuel cell. High output was obtained by directly employing the anode in undiluted high-temperature hydrothermal fluids. In the flow of the hydrothermal fluids, abundant electron donors, such as H_2S and H_2, are continuously provided to the anode. We estimated the flow rate of the hydrothermal fluids from the C0014G vent as approximately 3.0 $L s^{-1}$, and it has the power potential of 2.6 kW (see the Supporting Information). These results provide the foundation for the development of HF–SW environmental fuel cells for future application on a larger scale and over longer time periods for the in situ generation of electricity. The utilization of an artificial hydrothermal vent has advantages for the HF–SW environmental fuel cell because it provides excellent accessibility to the discharge of high-temperature hydrothermal fluids with an ROV. In addition, the discharge fluxes of the hydrothermal fluids and the patterns of the artificial vents can be mechanically controlled,[12] and anodes in the HF–SW fuel cell with large surface areas can be installed into the pipes. To this end, the materials and structure of the electrodes should be optimized to improve power production. In addition, the operational durability of the fuel cell should be studied. It is hypothesized that microbial populations in which the electricity sustains energy metabolism and biomass production are present in deep-sea vent ecosystems.[11] Some of these microbial populations might be able to catalyze the cathodic reaction of the HF–SW fuel cell and be enriched on the cathode surface. The investigation of these electrotrophic microorganisms and communities will provide important insights into extracellular electron transport in deep-sea hydrothermal environments.[7,11,15,16]

Experimental Section

Deep-sea electrochemical analyses: The deep-sea potentiostat system (D-Pote) was employed for the analyses. The working electrode was

a platinum disk 3 mm in diameter, and the circumference was coated with resin. The working electrode was fixed in a perforated stainless-steel pipe without electric contact. This pipe was hung on a hook in front of the ROV and maneuvered by the manipulator. A platinum rod was employed as the counter electrode. The reference electrode was a silver chloride electrode in a saturated potassium chloride solution. The counter and reference electrodes were fixed next to the working electrode on the ROV.

Construction of the HF–SW fuel cell: A platinum mesh board was employed as the cathode. The anode consisted of a titanium pipe in which iridium mesh boards were fitted. These electrodes were connected to D-Pote or a light-emitting diode (LED) lamp through underwater cables. The LED lamp consisted of a parallel circuit of three sets of a red LED with a boost DC-DC power converter. All of the LED-lamp components were sealed with epoxy resin.

Laboratory electrochemical analyses: A platinum and silver chloride electrode were employed as the counter and reference electrodes, respectively. Three types of plate electrodes (platinum, iridium, and chimney mineral) were employed as the working electrodes. The electrolytes contained NaCl (0.6 M) in the presence and absence of Na_2S (0.1 M). Both electrolytes were adjusted to a pH value of 8.0. The scan rate was 10 $mV s^{-1}$, and the scan direction was from a negative to a positive potential for the linear sweep voltammetry. See the Supporting Information for details.

Received: April 2, 2013
Revised: June 24, 2013
Published online: September 2, 2013

Keywords: electrochemistry · electrolytes · fuel cells · mineralogy · redox chemistry

[1] R. H. Charlier, *Renewable Sustainable Energy Rev.* **2003**, *7*, 515.
[2] G. Hiriart, I. a. Hernández, *GRC Trans.* **2010**, *34*, 1033.
[3] W. Griekspoor, *Resour. Conserv.* **1981**, *7*, 49.
[4] E. F. DeLong, P. Chandler, *Nat. Biotechnol.* **2002**, *20*, 788.
[5] C. R. German, L. L. Von Damm in *Treatise on Geochemistry, Vol. The Oceans and Marine Geochemistry* (Ed.: H. Elderfield), Elsevier, Amsterdam, **2006**, p. 181.
[6] K. Takai, K. Nakamura in *Geomicrobiology: Molecular and Environmental Perspective* (Eds.: L. L. Barton, M. Mandl, A. Loy), Springer, Dordrecht, **2010**, p. 251.
[7] R. Nakamura, T. Takashima, S. Kato, K. Takai, M. Yamamoto, K. Hashimoto, *Angew. Chem.* **2010**, *122*, 7858; *Angew. Chem. Int. Ed.* **2010**, *49*, 7692.
[8] K. Takai, M. J. Mottl, S. H. H. Nielsen, *Sci. Drill.* **2012**, *13*, 19.
[9] S. Kawagucci, H. Chiba, J. Shibash, T. Yamanaka, T. Toki, Y. Muramatsu, Y. Ueno, A. Makabe, K. Inoue, N. Yoshida, S. Nakagawa, T. Nunoura, K. Takai, N. Takahata, Y. Sano, T. Narita, G. Teranishi, H. Obata, T. Gamo, *Geochem. J.* **2011**, *45*, 109.
[10] J. W. Johnson, E. H. Oelkers, H. C. Helgeson, *Comput. Geosci.* **1992**, *18*, 899.
[11] P. R. Girguis, J. F. Holden, *Oceanography* **2012**, *25*, 213.
[12] M. E. Nielsen, C. E. Reimers, H. K. White, S. Sharma, P. R. Girguis, *Energy Environ. Sci.* **2008**, *1*, 584.
[13] M. K. Tivey, *Oceanography* **2007**, *20*, 50.
[14] K. Takai, T. Nunoura, J. I. Ishibashi, J. Lupton, R. Suzuki, H. Hamasaki, Y. Ueno, S. Kawagucci, T. Gamo, Y. Suzuki, H. Hirayama, K. Horikoshi, *J. Geophys. Res. Biogeosci.* **2008**, *113*, G02031.
[15] C. Pfeffer, S. Larsen, J. Song, M. Dong, F. Besenbacher, R. L. Meyer, K. U. Kjeldsen, L. Schreiber, Y. A. Gorby, M. Y. El-Naggar, K. M. Leung, A. Schramm, N. Risgaard-Petersen, L. P. Nielsen, *Nature* **2012**, *491*, 218.
[16] T. Mogi, T. Ishii, K. Hashimoto, R. Nakamura, *Chem. Commun.* **2013**, *49*, 3967.